AFRL-RQ-WP-TP-2014-0113

EXPLORATION OF NEAR-FIELD PLUME PROPERTIES FOR AERATED-LIQUID JETS USING X-RAY RADIOGRAPHY (POSTPRINT)

Kuo-Cheng Lin

Taitech, Inc.

Campbell Carter and Stephen Smith

Hypersonic Sciences Branch
High Speed Systems Division

Alan Kastengren

Argonne National Laboratory

FEBRUARY 2014

AIR FORCE RESEARCH LABORATORY
AEROSPACE SYSTEMS DIRECTORATE
WRIGHT-PATTERSON AIR FORCE BASE, OH 45433-7542
AIR FORCE MATERIEL COMMAND
UNITED STATES AIR FORCE

NOTICE AND SIGNATURE PAGE

Using Government drawings, specifications, or other data included in this document for any purpose other than Government procurement does not in any way obligate the U.S. Government. The fact that the Government formulated or supplied the drawings, specifications, or other data does not license the holder or any other person or corporation; or convey any rights or permission to manufacture, use, or sell any patented invention that may relate to them.

This report was cleared for public release by the USAF 88th Air Base Wing (88 ABW) Public Affairs Office (PAO) and is available to the general public, including foreign nationals.

Copies may be obtained from the Defense Technical Information Center (DTIC) (http://www.dtic.mil).

AFRL-RQ-WP-TP-2014-0113 HAS BEEN REVIEWED AND IS APPROVED FOR PUBLICATION IN ACCORDANCE WITH ASSIGNED DISTRIBUTION STATEMENT.

*//Signature//

CAMPBELL D. CARTER
Program Manager
Hypersonic Sciences Branch
High Speed Systems Division

//Signature//

RODOLFO G. BUENTELLO, Chief
Hypersonic Sciences Branch
High Speed Systems Division
Aerospace Systems Directorate

//Signature//

ROBERT A. MERCIER, Deputy for Technology
Aerospace Systems Directorate
High Speed Systems Division

This report is published in the interest of scientific and technical information exchange, and its publication does not constitute the Government's approval or disapproval of its ideas or findings.

*Disseminated copies will show "//Signature//" stamped or typed above the signature blocks.

REPORT DOCUMENTATION PAGE

Form Approved
OMB No. 0704-0188

1. REPORT DATE *(DD-MM-YY)*	2. REPORT TYPE	3. DATES COVERED *(From - To)*
February 2014	Conference Paper Postprint	01 October 2012 – 01 February 2014

4. TITLE AND SUBTITLE
EXPLORATION OF NEAR-FIELD PLUME PROPERTIES FOR AERATED-LIQUID JETS USING X-RAY RADIOGRAPHY (POSTPRINT)

5a. CONTRACT NUMBER
In-house

5b. GRANT NUMBER

5c. PROGRAM ELEMENT NUMBER
61102F

6. AUTHOR(S)
Kuo-Cheng Lin (Taitech, Inc.)
Campbell Carter and Stephen Smith (AFRL/RQHF)
Alan Kastengren (Argonne National Laboratory)

5d. PROJECT NUMBER
3002

5e. TASK NUMBER
N/A

5f. WORK UNIT NUMBER
Q0VH

7. PERFORMING ORGANIZATION NAME(S) AND ADDRESS(ES)
Taitech, Inc.
Beavercreek, OH 45430

Argonne National Laboratory
Argonne, IL 60439

Hypersonic Sciences Branch (AFRL/RQHF)
High Speed Systems Division
Air Force Research Laboratory, Aerospace Systems Directorate
Wright-Patterson Air Force Base, OH 45433-7542
Air Force Materiel Command, United States Air Force

8. PERFORMING ORGANIZATION REPORT NUMBER
AFRL-RQ-WP-TP-2014-0113

9. SPONSORING/MONITORING AGENCY NAME(S) AND ADDRESS(ES)
Air Force Research Laboratory
Aerospace Systems Directorate
Wright-Patterson Air Force Base, OH 45433-7542
Air Force Materiel Command
United States Air Force

10. SPONSORING/MONITORING AGENCY ACRONYM(S)
AFRL/RQHF

11. SPONSORING/MONITORING AGENCY REPORT NUMBER(S)
AFRL-RQ-WP-TP-2014-0113

12. DISTRIBUTION/AVAILABILITY STATEMENT
Approved for public release; distribution unlimited.

13. SUPPLEMENTARY NOTES
PA Case Number: 88ABW-2013-5129; Clearance Date: 03 Dec 2013.

The conference paper was presented at the 52nd Aerospace Sciences Meeting, held in National Harbor, Maryland, from January 13 through 17, 2014 and was published by AIAA SciTech as a part of the AIAA Aerospace Sciences Meeting (paper no. 2014-1183).

14. ABSTRACT
Near-field structures of aerated-liquid jets discharged from specially contoured exit adapters were explored, using the plume properties derived from synchrotron X-ray radiography. A total of six adapters with various internal contours were selected for testing. Water and nitrogen were used as the injectant and aerating gas, respectively. It was demonstrated that the liquid-weighted plume properties, including density, velocity, and momentum flux, within the cross-sectional planes perpendicular to the jet axis can provide useful insights to the understanding of aerated-liquid jets. For the adapters with a typical straight contour, pressure drop plays a role in determining the macroscopic spray structures of aerated-liquid jets at a given injection condition. A long passage length leads to a greater pressure drop and a reduced exit pressure to expand the plume diameter. For the adapter with a convergent-divergent contour, the jet properties are strongly affected by the exit slope of the adapter contour. An increase in aeration can substantially increase the plume velocity and plume momentum flux with no increase in spray cone angle.

15. SUBJECT TERMS

16. SECURITY CLASSIFICATION OF:			17. LIMITATION OF ABSTRACT:	18. NUMBER OF PAGES	19a. NAME OF RESPONSIBLE PERSON (Monitor)
a. REPORT	b. ABSTRACT	c. THIS PAGE			Campbell D. Carter
Unclassified	Unclassified	Unclassified	SAR	24	19b. TELEPHONE NUMBER *(Include Area Code)* N/A

AIAA SciTech
13-17 January 2014, National Harbor, Maryland
52nd Aerospace Sciences Meeting

Exploration of Near-Field Plume Properties for Aerated-Liquid Jets Using X-Ray Radiography

Kuo-Cheng Lin[a]
Taitech, Inc.
Beavercreek, Ohio 45430

Campbell Carter[b], Stephen Smith[c]
Air Force Research Laboratory, Aerospace Systems Directorate
Wright-Patterson AFB, Ohio 45433

Alan Kastengren[d]
Argonne National Laboratory
Argonne, Illinois 60439

ABSTRACT

Near-field structures of nominally axisymmetric aerated-liquid jets discharged from specially contoured exit adaptors were explored, using the plume properties derived from synchrotron X-ray radiography measurements. A total of six adaptors with various internal configurations and lengths were selected for testing. Water and nitrogen were used as the injectant and aerating gas, respectively. It was demonstrated that the liquid-weighted plume properties, including density, velocity, and momentum flux, within the cross-sectional planes perpendicular to the jet axis can provide useful insights to the understanding of aerated-liquid jets. For the conditions tested, it was found that the margin of benefit for liquid aeration diminishes for highly-dispersed aerated-liquid jets. For the adaptors with a typical straight contour, pressure drop across the adaptor plays a role in determining the macroscopic spray structures of aerated-liquid jets at a given injection condition. A long passage length leads to a greater pressure drop and, consequently, a reduced exit pressure to expand the plume diameter. For the adaptor with a convergent-divergent contour, the plume properties of aerated-liquid jets are strongly affected by the exit slope of the adaptor contour. An increase in aeration level can substantially increase the plume velocity and plume momentum flux with no increase in spray cone angle for the aerated-liquid jets discharged from the convergent-divergent adaptor. The adaptor with a convergent-only contour can efficiently generate highly-dispersed aerated-liquid jets without excessive pressure drops across the passage length.

NOMENCLATURE

D = diameter
D(y) = chord length through the plume cross section
d(x) = plume diameter at axial location x
D1 = entrance diameter
D2 = throat diameter
EPL = equivalent path length
GLR = aerating gas-to-liquid mass ratio
I = intensity of the transmitted light
I_0 = intensity of the incident light
L = passage length
m_L = liquid mass flow rate
r = radial position from the jet axis
TIM = time-averaged integrated liquid mass across the spray plume
u(x) = weighted plume velocity at axial location *x*
x = axial position from the injector exit; also X-ray beam path length
y = transverse position from the injector axis
α = linear attenuation coefficient
β = mass attenuation coefficient
Δy = X-ray transverse probing interval
ρ = density
ρ_{water} = water density, 1000 kg/m^3 or 1.0 g/cm^3
$\rho(y)$ = density along the beam path at transverse location *y*
$\rho(x)$ = weighted plume density at axial location x

INTRODUCTION

Liquid jet atomization plays an important role in establishing stable and efficient combustion inside the combustor of a liquid-fueled air-breathing propulsion system. For applications requiring both deep fuel penetration

[a] Senior Research Scientist, 1430 Oak Court, Suite 301, Beavercreek, OH 45430, Associate Fellow AIAA, corresponding author, Kuocheng.Lin.ctr@us.af.mil
[b] Principal Aerospace Engineer, AFRL/RQHF, Associate Fellow AIAA
[c] Aerospace Engineer, AFRL/RQHF, Member AIAA
[d] Physicist, Advanced Photon Source

into high-speed crossflows for broader fuel spreading and smaller droplets in the liquid spray for faster evaporation, a superior liquid injection scheme is sought. Among the possible candidates, aerated-liquid (also known as effervescent or barbotage) jets have been explored extensively. It has been shown that the liquid aeration technique can generate a spray that penetrates well into the flow and produces a large fuel plume containing a large number of small droplets.[1,2] The required amount of aerating gas and delivery pressure are practically obtainable in a high-speed air-breathing propulsion system. The utilization of aerated-liquid jets has led to successful combustion in a liquid-fueled high-speed air-breathing combustor.[3]

While macroscopic and far-field features of the aerated-liquid jets have been extensively examined, detailed near-field spray structures cannot easily be explored, due to instrumentation difficulties. The relatively dense spray structure of an aerated-liquid jet prohibits the use of conventional shadowgraph imaging and/or phase Doppler particle analyzer (PDPA). The holographic technique exhibits limited success in measuring droplet size and velocity in the vicinity of the near-field jet.[4] Recently, X-ray phase contrast imaging (PCI) technique, available at the Argonne National Laboratory, was successfully utilized to characterize dense diesel sprays and aerated-liquid jets.[5-9]

The study of Lin et al.[8] showed that an aerated-liquid jet with a modest aeration level can quickly disperse droplets and ligaments within the near field of the spray. Attempts to measure droplet diameter, bubble diameter, and bubble film thickness were also made in that study. Due to the line-of-sight feature of PCI, however, only the periphery of the spray can be probed for size measurement. The structure within the dense core region is still fairly inaccessible.[9] In addition, the PCI images cannot provide answers to whether the near-field structure of the discharged jet is co-annular or uniform in density. Several studies have reported co-annular structures within the aerated-liquid injectors.[10-13] The study of Lin et al.[8] proposes uniform homogeneous-like structure as the dominant two-phase structure within the aerated-liquid injectors. More recently, the study of Lin et al.[14] showed that the X-ray radiography can provide quantitative liquid mass distribution measurements within the dense near-field region of an aerated-liquid jet discharged from specially contoured adaptors.

The objective of the present study is to expand the study of Lin et al.[14] by examining liquid-based plume properties, such as averaged density, velocity, and momentum flux, using the already-acquired X-ray radiography data sets for property derivation. Axial distribution profiles of plume properties were then compared to identify the effects of liquid flow rate, liquid aeration level, and adaptor contours on the near-field structures of aerated-liquid jets. Combination of the present study with previous studies with the X-ray techniques should give a better understanding of the aerated-liquid jets.

EXPERIMENTAL METHODS

The experiment was conducted at the 7-BM beamline of the Advanced Photon Source (APS) at Argonne National Laboratory. Water and nitrogen were supplied into the aerated-liquid injector at desired flow rates to form a two-phase mixture inside the injector before discharge into a quiescent environment. An axisymmetric aerated-liquid injector with an internal diameter of 2.0 mm in the mixing chamber was designed, as shown in Fig. 1. An adaptor with a specific internal contour, as shown in Fig. 2, can be mounted at the exit of the 2-mm injector to provide the desired transition from the 2.0 mm injector exit to a throat diameter of 1.0 mm. These contour profiles provide additional means to modify the two-phase mixture before the mixture discharges into a quiescent environment. Two sets of adaptors with lengths of 2.5 mm (L/D=2.5) and 10.0 mm (L/D=10) were tested to explore the effects of passage length and contour curvature on spray structure. More information regarding the experimental methods can be found in the study of Lin et al.[14]

For the present study, the water spray was placed in the path of a focused X-ray beam. The schematic in Fig. 3 illustrates the overall setup. The aerated-liquid jet was vertically discharged into a collecting bucket with a small opening on the cap to prevent stray droplets from entering the beam path. In addition, the distance between the nozzle exit and the bucket cap was kept around 15 mm, in order to avoid splashing. Both the aerated-liquid injector and the collecting bucket were rigidly mounted on a traversing table, which provided movement normal to the X-ray beam.

X-Ray Radiography

7-BM beamline is dedicated to time-resolved X-ray radiography and tomography experiments for fuel sprays and associated phenomena. The X-ray source for the beamline is a synchrotron bending magnet, which produces nearly collimated, broadband X-ray emission. The beamline consists of two radiation enclosures. The first enclosure

(7BM-A) houses a pair of slits to limit the X-ray beam size and a double multilayer monochromator (1.4% ΔE/E). The monochromatic beam then passes into the second radiation enclosure (7BM-B), which houses the experimental equipment. More information regarding the beamline performance can be found in Kastengren et al.[15]

For the current experiments, the X-ray photon energy was 6 keV. This provides a good compromise between absorption of the beam by the spray and excessive absorption by X-ray windows and ambient air. The beam was focused using a pair of 300 mm long Kirkpatrick-Baez focusing mirrors. The beam focus is approximately 5 × 6 μm FWHM V × H, located approximately 400 mm from the center of the horizontal focusing mirror. The effective size of the beam for the current sprays (which are several mm wide) is slightly greater than this minimum focus size due to beam divergence, but less than 20 μm throughout the spray.

The radiography measurements provide a quantitative measurement of the spray liquid density integrated along the beam path. Since the aerating gas (N_2) has nearly identical x-ray absorption to air, it is invisible to the radiography measurements. In order to build a two-dimensional representation of the spray, a raster scan approach is used, with individual measurements performed at multiple locations. As manipulation of the X-ray beam is difficult, the spray is placed on computer-controlled translation stages to perform the raster scanning. The X-ray detector for these experiments is an unbiased silicon PIN diode, 300 μm thick. This detector absorbs virtually all of the X-rays incident on the detector, converting the X-rays into a weak photocurrent. This current is amplified with a high-speed transimpedance amplifier, with the resulting voltage integrated for 1.0 s at each measurement location.

According to Beer's law, the relationship between the absorption of light and the properties of the material through which the light is travelling can be described as follows:

$$\frac{I}{I_0} = e^{-\alpha x} \tag{1}$$

where I and I_0 are the intensity of the transmitted light and the incident light, respectively, measured by the PIN diode, α is the linear attenuation coefficient, and x is the path length of the X-ray beam through the media of interest. For the present study, the media of interest is a multiphase flow consisting of air and a dispersed phase in the form of fine droplets and ligaments.

Equation (1) can be further manipulated as follows:

$$x \equiv EPL = \frac{-\ln\left(I/I_0\right)}{\alpha} = \frac{-\ln(I/I_0)}{\beta\rho} \tag{2}$$

where β is the mass attenuation coefficient and is equal to (α/ρ). For pure water at room temperature with a density of 1.0 g/cm^3 and mass attenuation coefficient of 24.19 cm^2/g at 6.0 keV without coherent scattering, the path length derived from Eq. (2) is the equivalent path length (EPL). The mass attenuation coefficient was calculated using the NIST photon cross sections database.[16] The equivalent path length is the thickness of pure water required for the transmitting X-ray to generate the same amount of extinction as that generated from the dispersed spray at the same X-ray energy level. The value of EPL can, therefore, be related to the local density of the liquid/air mixture or local liquid mass fraction. The two-dimensional line-of-sight EPL and the 2-D contours was presented in the study of Lin et al.[14] to depict the spray structure. In this study, no attempt was made to resolve the three-dimensional distribution of EPL through mathematical schemes such as Abel inversion.

Without measuring the properties of aerating gas within the aerated-liquid jet, the liquid-based plume properties can be calculated using the line-of-sight (LOS) EPL. Referring to the schematic in Fig. 4, the line-of-sight liquid density along each X-ray cord length within the plume cross section, $\rho(y)$, can be calculated as follows:

$$\rho(y) = \left(\frac{EPL}{D(y)}\right)\rho_{water} \tag{3}$$

where *D(y)* is the chord length through the plume cross section with the LOS EPL greater than 1.0 μm and ρ_{water} is the water density (1.0 g/cm^3 or 1000 Kg/m^3) at room temperature. The weighted plume density at each axial location, $\rho(x)$, can then be calculated as follows:

$$\rho(x) = \frac{\sum\{\rho(y)(D(y)\Delta y)\}}{\pi\left(\frac{d(x)}{2}\right)^2} = \frac{TIM}{\pi\left(\frac{d(x)}{2}\right)^2} \tag{4}$$

where Δy is the X-ray radial probing interval of the present study, *TIM* is the time-averaged integrated mass of the liquid found at a given x location (in units of mass/length in *x*), and *d(x)* is the diameter of spray cross section, defined as the region with the LOS EPL greater than 1.0 μm. It should be noted that this analysis for plume density assumes that the local, ensemble average density of liquid is uniform across the cross-section of the spray. This analysis could be improved by fitting the measured EPL distributions to account for non-uniformities in the liquid distribution, though no such fitting was attempted in this work. It should also be noted that the derived density is the local, time-averaged liquid density, and does not account for the gas density.

The weighted plume velocity, u(x), can be calculated from the continuity as follows:

$$u(x) = \frac{m_L}{\rho(x)\left\{\pi\left(\frac{d(x)}{2}\right)^2\right\}} = \frac{m_L}{TIM} \tag{5}$$

where m_L is the injected liquid flow rate for each test condition. This quantity represents the average velocity of the liquid integrated for all *y* at a given *x*. It is also weighted by the local density. The analysis for plume velocity does not depend on assumptions regarding the liquid density distribution.

RESULTS AND DISCUSSION

Spray Regime Map

Figure 5 is an adopted figure from the study of Lin et al.[14] to show the typical regime map in terms of liquid flow rate and gas-to-liquid mass ratio (GLR) for aerated-liquid jets. The Configuration #1 adaptor with L/D=10 was used. In Fig. 5, the executed injection conditions are represented with red symbols. Macroscopic appearances of corresponding sprays discharged into a quiescent environment were visualized using conventional photography and are placed next to the marked test conditions in Fig. 5. As can be seen in Fig. 5, well-dispersed sprays can only be achieved at a fairly high GLR for the operating condition with a low liquid flow rate. On the other hand, well-dispersed sprays can be obtained at a fairly low GLR for the operating condition with a high liquid flow rate. While this regime map is useful in understanding the macroscopic appearances of aerated-liquid jets at various operating conditions and can be helpful for some spray applications, these images do not provide quantitative measurements of relevant plume properties, such as the averaged density, velocity, and momentum flux.

Liquid Mass Distribution Profiles

Using this regime map in Fig. 5 as the reference, the effects of liquid mass flow rate on the structures of aerated-liquid jets at a given aeration level are shown in Fig. 6. This figure is adopted from the study of Lin et al.[14] The aeration level was fixed at 4% for four selected liquid flow rates from 4.5 g/s to 27.2 g/s. Transverse distribution profiles of the EPL also depict the evolution of the injected liquid mass along the jet axis from x=0.5 mm to 12.5 mm in Fig. 6.

A number of conclusions can be drawn from these figures. First of all, the spray width increases with liquid flow rate at a given aeration level. A higher injection pressure to discharge more fluid through the injector orifice is a plausible contributing mechanism. Second, the peak value of the equivalent path length at the x=0.5 mm location is significantly lower than the exit orifice diameter of 1.0 mm, indicating that the liquid volume fraction at the nozzle exit is considerably less than 1. Third, the aerated-liquid jets with liquid flow rates of 4.5 and 9.1 g/s (Figs. 6(a) and 6(b), respectively) exhibit a bimodal distribution, which indicates an annular flow of liquid, with more liquid distributed within an annular ring near the periphery of the jet. This means that the liquid and aerating gas are not well mixed, and much of the aerating gas inhabits the core region inside the injector. This annular flow feature

persists within the axial range of the measurements for both conditions. At higher liquid flow rates, the measured transverse distribution profiles for the EPL are far more Gaussian. This implies more uniform mixing between liquid and aerating gas at these liquid flowrates. The transition from annular-like flow to a well-dispersed flow takes place between liquid flow rates of 9.1 g/s to 18.2 g/s for this injector/adaptor assembly operated at GLR=4%.It should be stressed that these details regarding the liquid distribution could not be derived from Mie scattering or shadowgraph images of these sprays.

Plume Properties

Figure 7(a) shows the axial distribution of plume diameter, which is defined as the region with EPL greater than an arbitrarily chosen value of 1.0 μm. The plume diameter increases linearly with the axial locations for each test condition. Also, the plume diameter increases as liquid flow rate increases up to a certain value at the same aeration level. Both sprays with 18.2 and 27.2 g/s liquid flow rates exhibit nearly identical plume widths. For both well-dispersed sprays, the measured plume diameter exhibits some uncertainties, due to radial X-ray probing resolution (Δy), spray unsteadiness, and the gradual gradients in EPL at the edges of these sprays at the most downstream locations.

Axial distribution profiles of liquid-based plume density, calculated from Eq. (4), are shown in Fig. 7(b). Also shown in Fig. 7(b) are the fitting lines of the calculated density and the ambient air density for comparison. The weighted plume density decreases dramatically along the jet axis for each injection condition, due to the increase in plume diameter and the decrease in peak EPL. As the liquid flow rate increases, plume density decreases, due to a higher rate of expansion for the plume diameter. Once again, the sprays with 18.2 and 27.2 g/s liquid flow rates exhibit nearly identical distribution profiles for the plume density. At further downstream locations for both sprays, the calculated plume density is less than the ambient air density, indicating that the time-averaged liquid mass fraction has fallen below 0.5 in these locations. This observation highlights the need to include the gas phase properties for the calculation of averaged plume density for the aerated-liquid jets, even though the percentage of gas mass is relatively low.

In the axial profiles of the liquid-weighted plume velocity (Fig. 7c), the injected liquid gradually increases in velocity and then approaches an asymptotic average speed at the downstream locations for the injection conditions with low liquid flow rates. At high liquid flow rates, plume velocity initially increases and then decreases downstream. With almost identical distribution profiles for plume diameter and plume density for both sprays with 18.2 and 27.2 g/s liquid flow rates, the increase in liquid flow rate directly leads to a higher plume velocity. The qualitative differences between the low- and high-flowrate cases are likely directly tied to the differences in the liquid distribution shape. For the high-flowrate cases, the liquid and aerating gas are well mixed, leading to a wide jet with strong interactions with the ambient gas. For the low-flowrate cases, the co-annular structure leads to a narrower jet. It also seems likely that the central gas jet may move at substantially higher velocity than the liquid in these sprays, with shear against this gas counteracting the effects of drag from the quiescent ambient gas.

Figure 7(d) shows the distributions of the weighted liquid momentum flux, which is directly calculated from the plume density in Fig. 7(b) and the plume velocity in Fig. 7(c). It should be stressed that this measure of momentum flux is only approximate, as measurements of velocity and density as a function of y would be needed to rigorously calculate momentum flux. First of all, plume momentum flux decreases with the axial locations, mainly due to the increase in plume diameter for a reduced plume density. Second, with the same nozzle exit to discharge more liquid and aerating gas, plume momentum flux increases with liquid flow rate (at the same GLR) in the region immediately adjacent to the nozzle exit. Further downstream with x>10 mm, however, the derived momentum flux exhibits a higher value for both jets with lower liquid flow rates. Third, both well-dispersed sprays with liquid flow rate of 18.2 and 27.2 g/s lose momentum flux quickly along the jet axis, indicating intense momentum exchange (or mixing) between the plume and the ambient air. For both aerated-liquid jets with liquid flow rate of 4.5 and 9.1 g/s, however, a slower decrease in momentum flux along the jet axis is clearly observed, indicating limited momentum exchange with the ambient air for both jets.

In summary, X-ray radiography measurements along with the derived plume properties can provide a significant amount of information for the structures of the aerated-liquid jet within the near-field region. For the injection conditions described in Fig. 7, the aerated-liquid jets with well-dispersed plumes exhibit a wider plume diameter, a higher velocity, a lower density, and a higher momentum flux in the region adjacent to the nozzle exit (x<2 mm). When injected into a crossflow environment, the well-dispersed jets can penetrate deeper, due to the high

momentum flux, and mix with the ambient air faster, due to the large plume diameter. Interestingly, the weighted plume velocity for the well-dispersed jets gradually decreases from x=2 mm to x=10 mm and eventually leads to a fast decay in momentum flux.

Effects of Aeration Level

Figure 8 shows the axial distributions of plume properties for aerated-liquid jets with the aeration level varied from 2% to 8% at a constant liquid flow rate of 9.1 g/s. The Configuration #1 adaptor with L/D=10 was used. The corresponding spray appearances can be seen in the spray regime map (Fig. 5). The study of Lin et al.[14] indicates that the injected sprays for these injection conditions in Fig. 8 all exhibit annular-like flow structures within the plumes. The present measurements show that the plume diameter, or spray cone angle, increases as the aeration level increases, due to the increase in injection pressure to assist plume dispersion, in Fig. 8(a). The derived plume properties further indicate that the weighted plume density decreases as the aeration level increases, due to the increase in plume diameter, as illustrated in Fig. 8(b). The weighted plume velocity for both jets with GLR=6% and 8% in Fig. 8(c) exhibit an initial increase within the region with x<2 mm and then gradually decreases toward downstream locations. Surprisingly, the derived momentum flux for the high aeration cases is smaller than that for the low aeration cases within the X-ray probing range in Fig. 8(d). The injection condition with a high aeration level has a higher total injected mass and a higher injection pressure, which is unexpected. The lack of the inclusion of aeration gas momentum, which can be fairly high at a high GLR injection condition, may account for this behavior.

Similar plots for the injection conditions with the constant liquid flow rate elevated from 9.1 g/s to 18.2 g/s are shown in Fig. 9, using the same Configuration #1 adaptor with L/D=10. Due to the constraints from the injection system, the aeration level beyond 6% could not be achieved. The corresponding spray appearances can be found in Fig. 5. The study of Lin et al.[14] indicates that the injected sprays for these injection conditions in Fig. 9 exhibit Gaussian-like or uniform flow structures within the plumes. The axial distribution profiles of the weighted plume properties in both Fig. 8 and Fig. 9, however, do not exhibit any distinct features to reflect the differences between annular- and Gaussian-like liquid mass distributions within the injected plumes. The axial distribution profiles for the injection condition with GLR=6% exhibits a higher degree of scattering in Fig. 9, due to the presence of drifted fine water mist for the highly-dispersed plume. In general, an increase in aeration level for an aerated-liquid jet at an elevated liquid flow rate can result in plume diameter increase, plume density decrease, and initial plume velocity increase. The weighted velocity for an aerated-liquid jet with limited dispersion exhibits an initial increase and then approaches an asymptotic value along the plume axis. For a well-dispersed aerated-liquid jet, the weighted plume velocity exhibits an initial increase, followed by a steep decrease along the jet axis. Without considering the gas phase properties, both Fig. 8 and Fig. 9 show that a further increase in aeration level from GLR=6% to 8% or higher at a constant liquid flow rate can only create marginal benefits in terms of macroscopic plume properties.

Effects of Adaptor Configuration

The effects of adaptor configuration on plume properties are shown in Fig. 10. The two-phase mixture with a liquid flow rate of 18.2 g/s and a GLR of 2% was injected through the selected adaptors. Each adaptor has an L/D of 2.5. As can be seen in Fig. 10, the spray plumes discharged from both Configuration #1 and Configuration #3 have the similar distribution profiles. The plume from the Configuration #3 adaptor, however, has a wider plume diameter and, consequently, a lower weighted liquid density, a lower weighted velocity, and a lower momentum flux. The study of Lin et al.[14] shows that a higher effective injection pressure for the aerated-liquid injected from the Configuration #3 adaptor is the contributing factor. With a gradual converging contour for the Configuration #3 adaptor, the pressure drop across the adaptor is smaller than that for the Configuration #1 adaptor. A higher pressure drop across the nozzle exit plane of the Configuration #3 adaptor can, therefore, create a larger expansion for the discharged aerated-liquid jets.

The plume properties for the aerated-liquid jet discharged from the Configuration #2 adaptor exhibit different features in distribution profiles in Fig. 10. With an exit orifice diameter of 2 mm for the Configuration #2 adaptor, due to the specially-designed convergent-divergent (C-D) contour, the discharged plume has a wider initial diameter at the exit plane and then undergoes a slower rate of growth for the plume diameter in Fig. 10(a). The study of Lin et al.[14] shows that the spray cone angle agrees fairly well with the exit slope of the Configuration #2 adaptor contour with an L/D of 2.5. It was also postulated by Lin et al.[14] that the two-phase mixture, which may possess a low speed of sound, is choked at the throat of the Configuration #2 adaptor. The continuous expansion of the two-phase mixture between the divergent sections of the adaptor eventually leads to a reduced or no pressure drop across the nozzle exit plane. Consequently, the discharged plume follows the exit slope of the adaptor contour without further

lateral expansion, as illustrated in Fig. 10(b). With a smaller plume diameter or spray cone angle, the weighted density is expected be higher at the downstream locations for the plume injected from the Configuration #2 adaptor. The calculated plume velocity quickly reaches an asymptotic value within 4 mm from the nozzle exit plane, indicating limited plume dispersion for the aerated-liquid discharged from the Configuration #2 adaptor in Fig. 10(c). The relatively high plume density is the main factor in preserving the momentum flux at the downstream locations for this aerated-liquid jet.

Effects of Adaptor Length (L/D)

Figure 11 shows the plume properties for the aerated-liquid jets injected from all three adaptors with an L/D of 10 at the injection condition same as that used in Fig. 10. Therefore, Fig. 11 can be compared with Fig. 10 to illustrate the effects of adaptor length, or L/D, on plume properties. The most obvious observation is that the long adaptor length (or L/D) can reduce the diameters of spray plumes discharged from both Configuration #1 and Configuration #2 adaptors. For Configurations #1, the reduction in plume diameter comes from the increase in pressure drop across the L/D=10 adaptor, resulting in a reduced pressure drop across the nozzle exit plane for lateral spray expansion. For Configuration #2, however, the reduction in plume diameter comes from the expansion processes of the compressible two-phase mixture across the C-D contour and the reduction in exit slope for the L/D=10 adaptor. The reduction in exit slope can be seen in the corresponding adaptor schematics Fig. 2. With a reduced plume diameter for the aerated-liquid jet discharged from the Configuration #2 adaptor with an L/D of 10, the weighted plume density, velocity, and momentum flux increase accordingly in Fig. 11, as expected. The spray plume discharged from the Configuration #1 adaptor exhibits similar reduction in plume density and momentum flux for the long L/D adaptor. The weighted plume velocity, however, shows a slight difference in the region with $x<4$ mm between both L/D=2.5 and L/D=10 adaptors. The jet discharged from the Configuration #1 adaptor with L/D=2.5 exhibits a larger increase in weighted plume velocity with this region. Experimental uncertainties or nature of the expansion processes within the region adjacent to the nozzle exit can be the contributing factor and should be explored in the future. In the region with $x>4$ mm, the weighted plume velocity is almost the same for both adaptor lengths. Interestingly, the plume properties are not significantly affected by the adaptor length for the #3 configuration in the present study. The highly-dispersed plumes, however, lead to higher measurement uncertainties, due to drifted fine mist especially at the downstream locations. For applications requiring a long L/D for the aerated-liquid injectors, the discharge passage with a converging contour can be a plausible solution to mitigate the degradation in plume properties or the need of an elevated delivery pressure to overcome the excessive pressure drop across the long discharge passage.

Plume Properties from C-D Adaptor

The unique features of the spray plumes generated from the Configuration #2 adaptors were selected for further discussion in this paper. Figure 12 shows the plume properties derived from the X-ray radiography measurements for aerated-liquid jets at a constant liquid flow rate of 18.2 g/s, two aeration levels (GLR=2% and 4%), and two adaptor lengths (L/D=2.5 and 10). The results show that the rate of growth for plume diameter, or the spray cone angle, is totally determined by the exit slope of the adaptor contour, as discussed previously. The adaptor with an L/D of 2.5 can generate a wider plume for the aerated-liquid jet. The change of aeration level from 2% to 4% has no impact to the plume diameter for a given adaptor length, even though a higher injection pressure is typically required to deliver the jet with GLR=4%. As the aeration level increases for a given adaptor length, the weighted plume density decreases, indicating a lower liquid volume fraction within the two-phase mixture. Figure 12 also shows that the plume density increases as the plume diameter decreases for the jets discharged from the L/D=10 adaptor at the same injection condition. For the injection condition shown in Fig. 12, an increase of around 50% to 60% in weighted plume velocity and weighted momentum flux can be achieved by a small increase of aeration level from 2% to 4% for both adaptor lengths. In general, the macroscopic features of the aerated-liquid jets can be manipulated by adjusting the C-D contour in terms of adaptor length and the ratio between throat diameter and the exit diameter, if the primary interest is not in the generation of highly-dispersed jets.

CONCLUSIONS

Near-field properties of aerated-liquid jets discharged from specially contoured exit adaptors were studied, using liquid-weighted plume properties derived from X-ray radiography measurements. The use of a synchrotron x-ray source with a monochromatic beam allowed for a simple conversion of x-ray intensity to liquid pathlength. Water and nitrogen were used as the injectant and aerating gas, respectively. An axisymmetric aerated-liquid injector equipped with an exit adaptor was utilized to deliver the aerated-liquid jets. A total of six adaptors with various internal configurations and lengths were selected for testing. The specific objective is to characterize the

plume diameter and averaged plume properties, such as density, velocity, and momentum flux, at various cross-sectional planes perpendicular to the jet axis for aerated-liquid jets at various injection conditions. Properties of aerating gas within the discharged plumes, however, were ignored in this study, due to the lack of gas phase measurement. Major findings of the present study are as follows:

1. The use of averaged spray plume properties, derived from the quantitative X-ray radiography measurements for liquid phase, has been successfully demonstrated to characterize the structures of aerated-liquid jets.

2. For adaptors with a straight passage:
   a) At a given aeration level, an increase in liquid flow rate leads to an increase in plume diameter and a reduction in weighted plume density. Both weighted plume velocity and plume momentum flux increase with the liquid flow rate in the region adjacent to the nozzle exit. For the highly-dispersed aerated-liquid jets generated from high liquid flow rates, both plume velocity and momentum flux decrease at the downstream locations, due to momentum exchange (or mixing) with the ambient air.

   b) At a given flow rate, an increase in aeration level leads to a wider spray plume, a reduced plume density, and a higher plume exit velocity. The highly-dispersed aerated-liquid jets generated from high aeration levels exhibits reductions in plume velocity and momentum flux as the plume is convected toward downstream.

   c) For the conditions tested, the margin of benefit for liquid aeration diminishes for highly-dispersed aerated-liquid jets. In the present study, GLR of 6% or 8% appears as the threshold aeration level.

3. Effects of adaptor contours:
   a) For the adaptors with a straight contour (Configuration #1): Pressure drop across the adaptor plays a role in determining the macroscopic spray structures of aerated-liquid jets. At the same injection condition, a long nozzle passage length leads to a greater pressure drop and, consequently, a reduced exit pressure to expand the spray plume, resulting in a reduction in plume diameter.

   b) For the adaptor with a convergent-divergent (C-D) contour (Configuration #2): The macroscopic plume properties of aerated-liquid jets are strongly affected by the exit slope of the adaptor contour. The rate of growth for the plume diameter, or the spray cone angle, is dictated by the exit slope. Injection pressure does not contribute to additional lateral plume expansion, due to the expansion processes of the compressible two-phase mixture within the adaptor to significantly reduce the plume exit pressure. At the same liquid flow rate for a given C-D adaptor, an increase in aeration level can substantially increase the plume velocity and plume momentum flux with no increase in spray cone angle.

   c) For the adaptor with a converging contour (Configuration #3): the general features of the macroscopic plume properties of aerated-liquid jets are similar to those generated from the adaptor with a straight contour. The converging contour, however, can reduce the pressure drop across the adaptor and consequently, leads to a higher plume exit pressure to generate a wider plume. In general, the divergent-only contour is more efficient in generating highly-dispersed aerated-liquid jets in terms of delivery pressure.

Due to the lack of gas phase property measurement for the derivation of averaged plume properties, the weighted plume density less than the ambient density is observed for the well-dispersed aerated-liquid jets in the present study. Future efforts to combine X-ray radiography for liquid phase measurement and X-ray fluorescence for gas phase measurement should be carried out to better characterize the plume structures.

ACKNOWLEDGEMENTS

This work was sponsored by the AFRL/Propulsion Directorate under contract number FA8650-08-D-2844 (Contract monitor: Stephen Smith) and by the Air Force Office of Scientific Research (AFOSR). Use of the Advanced Photon Source at Argonne National Laboratory was supported by the U. S. Department of Energy, Office of Science, Office of Basic Energy Sciences, under Contract No. DE-AC02-06CH11357. The authors would like to thank Matt Streby,

Steve Enneking, Timothy Bulcher (Taitech, Inc.) and Jaime Larios-Barbosa (AFRL) for their assistance in hardware design, setup, and data acquisition.

REFERENCES

1. Lin, K.-C., Kennedy, P. J., and Jackson, T. A., "Spray Structures of Aerated-Liquid Jets in Subsonic Crossflows," AIAA Paper 2001-0330, 2001.
2. Lin, K.-C., Kennedy, P. J., and Jackson, T. A., "Structures of Aerated Liquid Jets in High Speed Crossflows," AIAA Paper 2002-3178, 2002.
3. Mathur, T., Lin, K.-C., Kennedy, P., Gruber, M., Donbar, J., Jackson, T., and Billig, F., "Liquid JP-7 Combustion in a Scramjet Combustor," AIAA Paper 2000-3581, 2000.
4. Sallam, K. A., Aalburg, C., Faeth, G. M., Lin, K.-C., Carter, C. D., and Jackson, T. A., "Primary Breakup of Round Aerated-Liquid Jets in Supersonic Crossflows," *Atomization and Sprays*, Vol. 16, No. 6, 2006, pp. 657–672.
5. Wang, Y., Liu, X., Im, K.-S., Lee, W.-K., Wang, J., Fezzaa, K., Hung, David, and Winkelman, J., "Ultrafast X-Ray Study of Dense Liquid Jet Flow Dynamics Using Structure Tracking Velocimetry," *Nature Physics*, Vol. 4, 2008, pp. 305-309.
6. Qun, S., Lee, W-K., Fezzaa, K., Chu, Y. S., De Carlo, F., Jemian, P., Ilavsky, J., Erdman, M., and Long, G., "Dedicated Full-Field X-Ray Imaging Beamline at Advanced Photon Source," *NIM A* 582 (1), 77-79 (2007).
7. Lin, K.-C., Carter, C., Fezzaa, K., Wang, J., Liu, Z., "X-Ray Study of Pure- and Aerated-Liquid Jets in a Quiescent Environment," AIAA Paper 2009-0994, January 2009.
8. Lin, K.-C., Rajnicek, C., McCall, J., Fischer, B., Carter, C., and Fezzaa, K., "Structures of Aerated-Liquid Jets Injected from Various Nozzle Contours," AIAA Paper 2011-0232, 2011.
9. Lin, K.-C., Rajnicek, C., McCall, J., Carter, C., and Fezzaa, K., "Investigation of Pure- and Aerated-Liquid Jets Using X-Ray Phase Contrast Imaging Technique," *Nuclear Instruments and Methods in Physics Research Section A*, Vol. 649, No. 1, 2011, pp. 194-196.
10. Kim, J. Y., and Lee, S. Y., "Dependence of Spraying Performance on the Internal Flow Pattern in Effervescent Atomizers," *Atomization and Sprays*, Vol. 11, 2001, pp. 735-756.
11. Lorcher M., Schmidt, F., and Mewes, D., "Effervescent Atomization of Liquids," *Atomization and Sprays*, Vol. 15, 2005, pp. 145-168.
12. Catlin, C. A., and Swithenbank, J., "Physical Processes Influencing Effervescent Atomizer Performance in the Slug and Annular Flow Regimes," *Atomization and Sprays*, Vol. 11, 2001, pp. 575-595.
13. Huang, X., Wang, X., and Liao, G., "Visualization of Two Phase Flow inside an Effervescent Atomizer," *Journal of Visualization*, Vol. 11, No. 4, 2008, pp. 299-308.
14. Lin, K.-C., Carter, C., Smith, S., and Kastengren, A., "Exploration of Aerated-Liquid Jets Using X-Ray Radiography," AIAA Paper 2012-0347, January 2012.
15. Kastengren, A. L., Powell, C. F., Arms, D., Dufresne, E., and Wang, J., "Spray Diagnostics at the Advanced Photon Source 7-BM Beamline," ILASS Americas, 22nd Annual Conference on Liquid Atomization and Spray Systems, Cincinnati, OH, May 2010.
16. Berger, M. J., Hubbell, J. H., Seltzer, S. M., Chang, J., Coursey, J. S., Sukumar, R., Zucker, D. S., and Olsen, K., XCOM: Photon Cross Sections Database, NIST Standard Reference Database 8 (XGAM), http://www.nist.gov/pml/data/xcom/index.cfm.

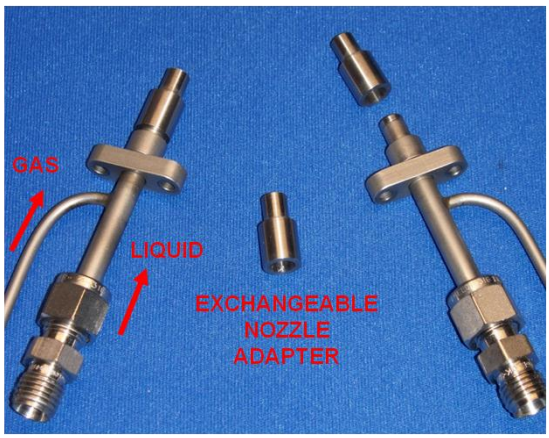

Figure 1. Photograph of axisymmetric aerated-liquid injector with exchangeable nozzle adaptors

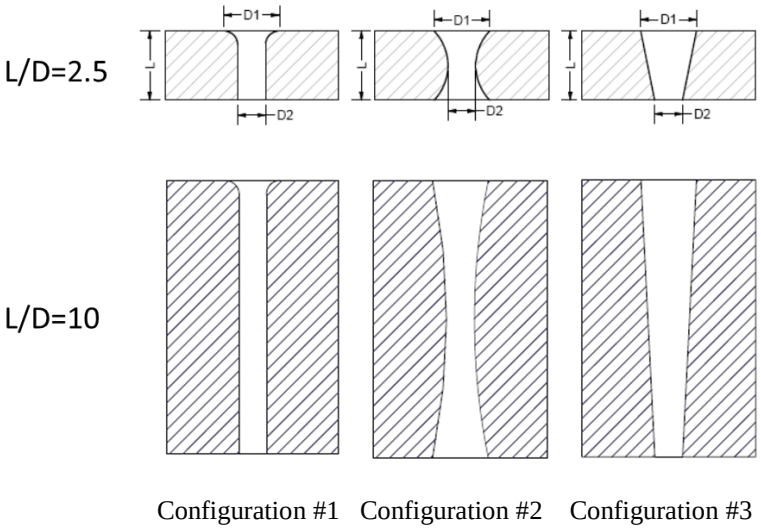

Figure 2. Adaptor internal contours for the axisymmetric aerated-liquid injector. D1=2.0 mm, D2=1.0 mm.

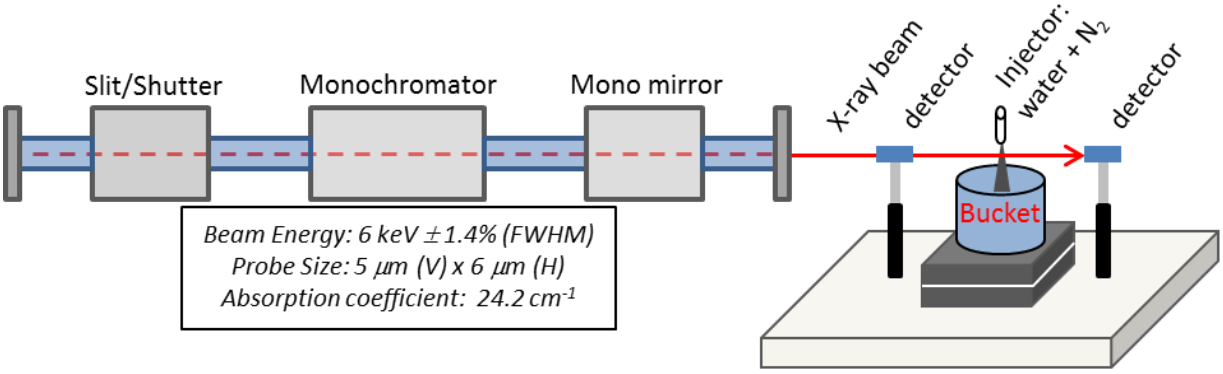

Figure 3. X-ray and injection stand setup at the 7-BM beamline at the Argonne National Laboratory.

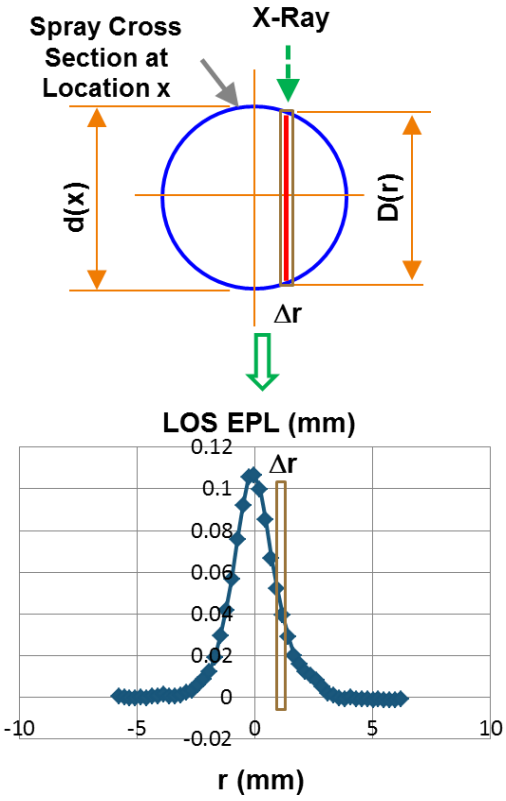

Figure 4. Schematic to show X-ray probing and the methodology for plume property calculations

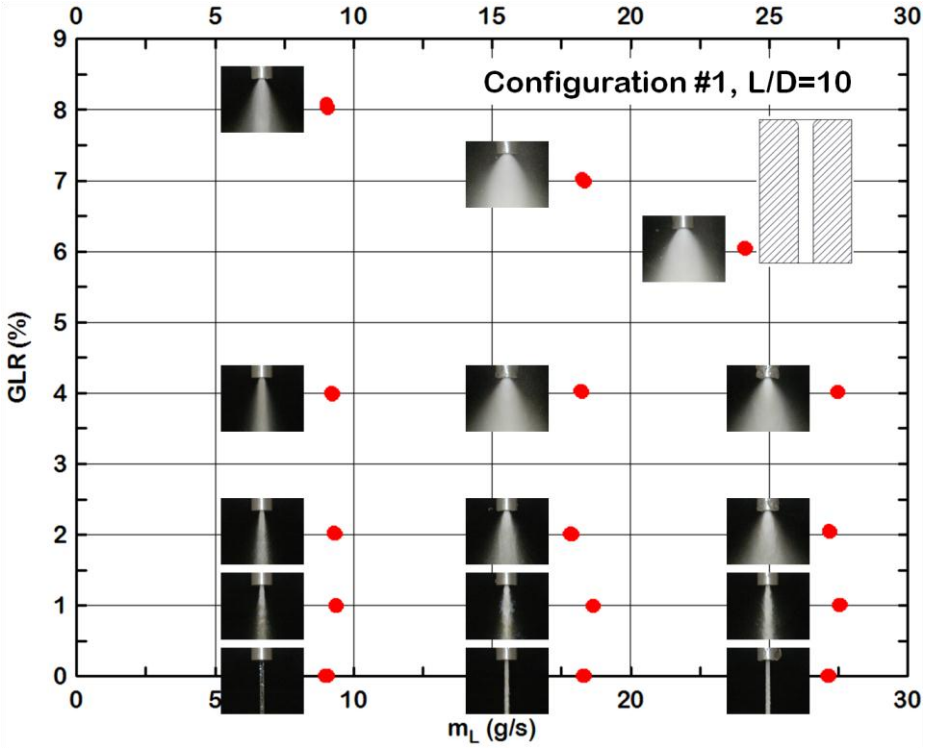

Figure 5. Regime maps showing the macroscopic structures of aerated-liquid jets at various liquid flow rates and aeration levels for the Configuration #1 adaptor with L/D=10. Adopted from Ref. [14].

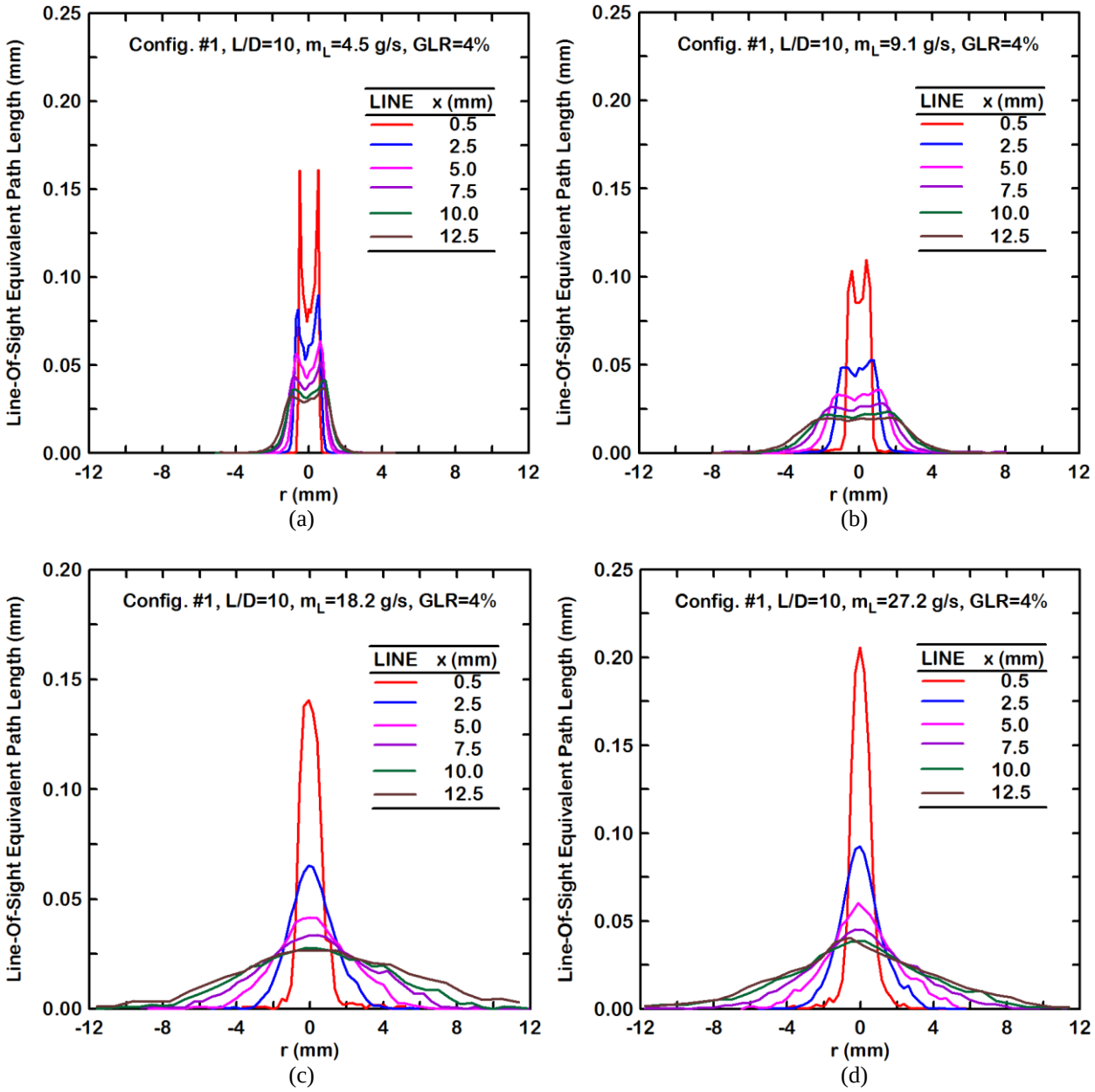

Figure 6. Radial distribution profiles of equivalent path length for aerated-liquid jets at various liquid flow rates. (a) m_L =4.5 g/s, (b) m_L =9.1 g/s, (c) m_L =18.2 g/s, (d) m_L =27.2 g/s. Configuration #1, L/D=10, GLR=4%. Adopted from Ref. [14].

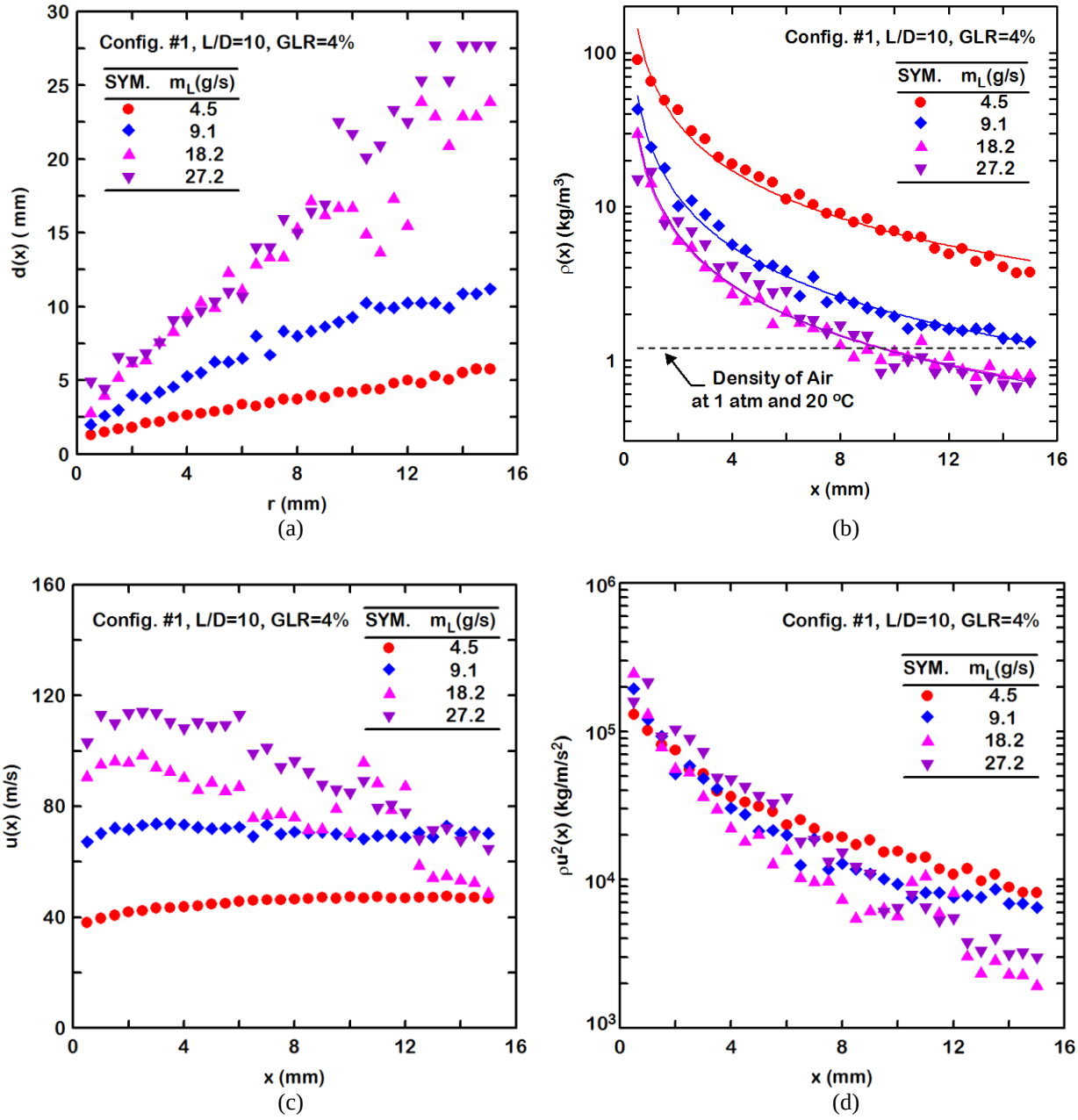

Figure 7. Axial distributions of (a) plume diameter, (b) weighted plume density, (c) weighted plume velocity, and (d) weighted momentum flux for aerated-liquid jets with various liquid flow rates at the same aeration level. The Plume diameter is defined as the region with LOS EPL greater than 1.0 μm. Configuration #1, L/D=10, GLR=4%.

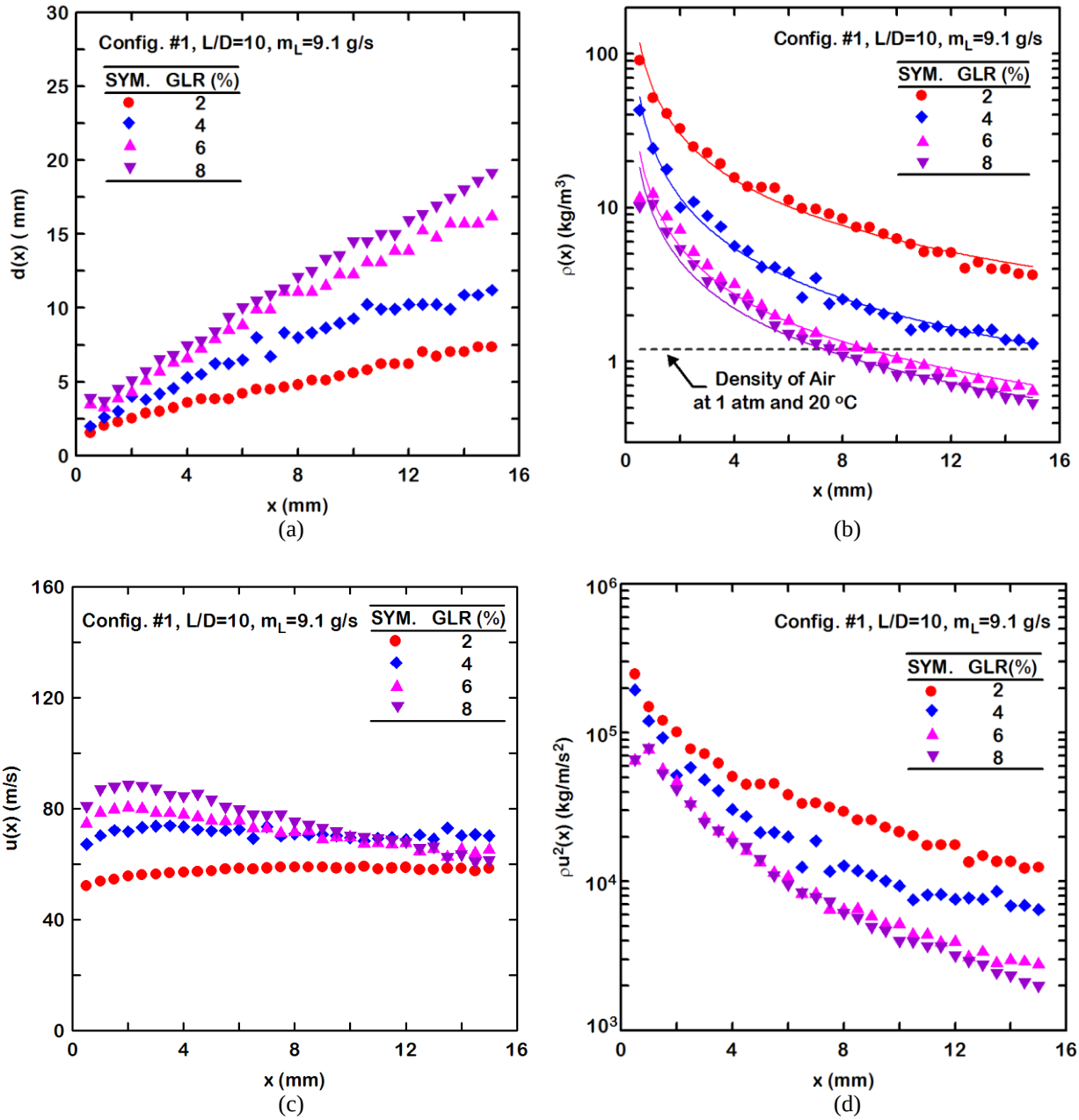

Figure 8. Axial distributions of (a) plume diameter, (b) weighted plume density, (c) weighted plume velocity, and (d) weighted momentum flux for aerated-liquid jets with various aeration levels at the same liquid flow rate. Configuration #1, L/D=10, m_L=9.1 g/s.

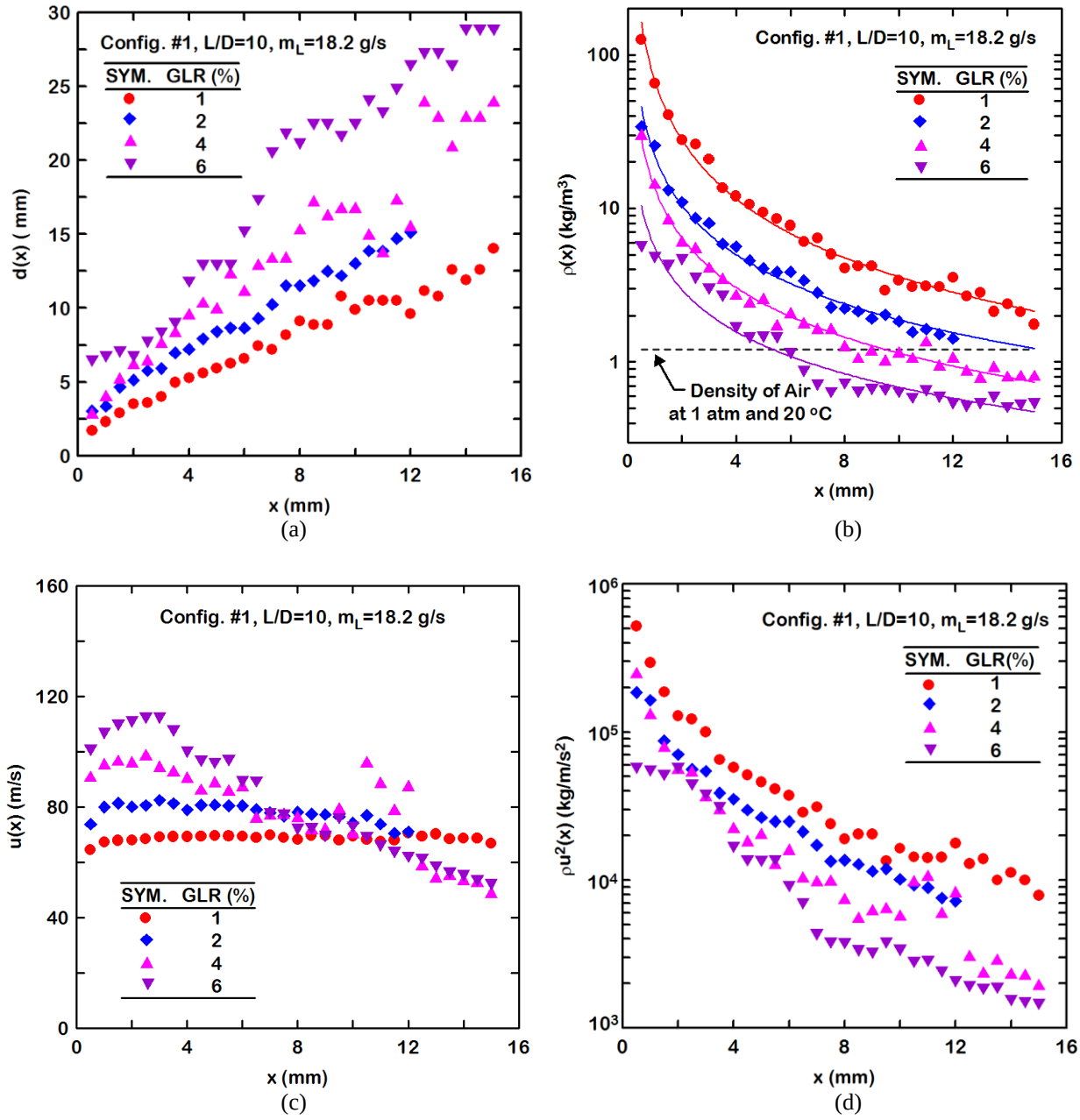

Figure 9. Axial distributions of (a) plume diameter, (b) weighted plume density, (c) weighted plume velocity, and (d) weighted momentum flux for aerated-liquid jets with various aeration levels at the same liquid flow rate. Configuration #1, L/D=10, m_L=18.2 g/s.

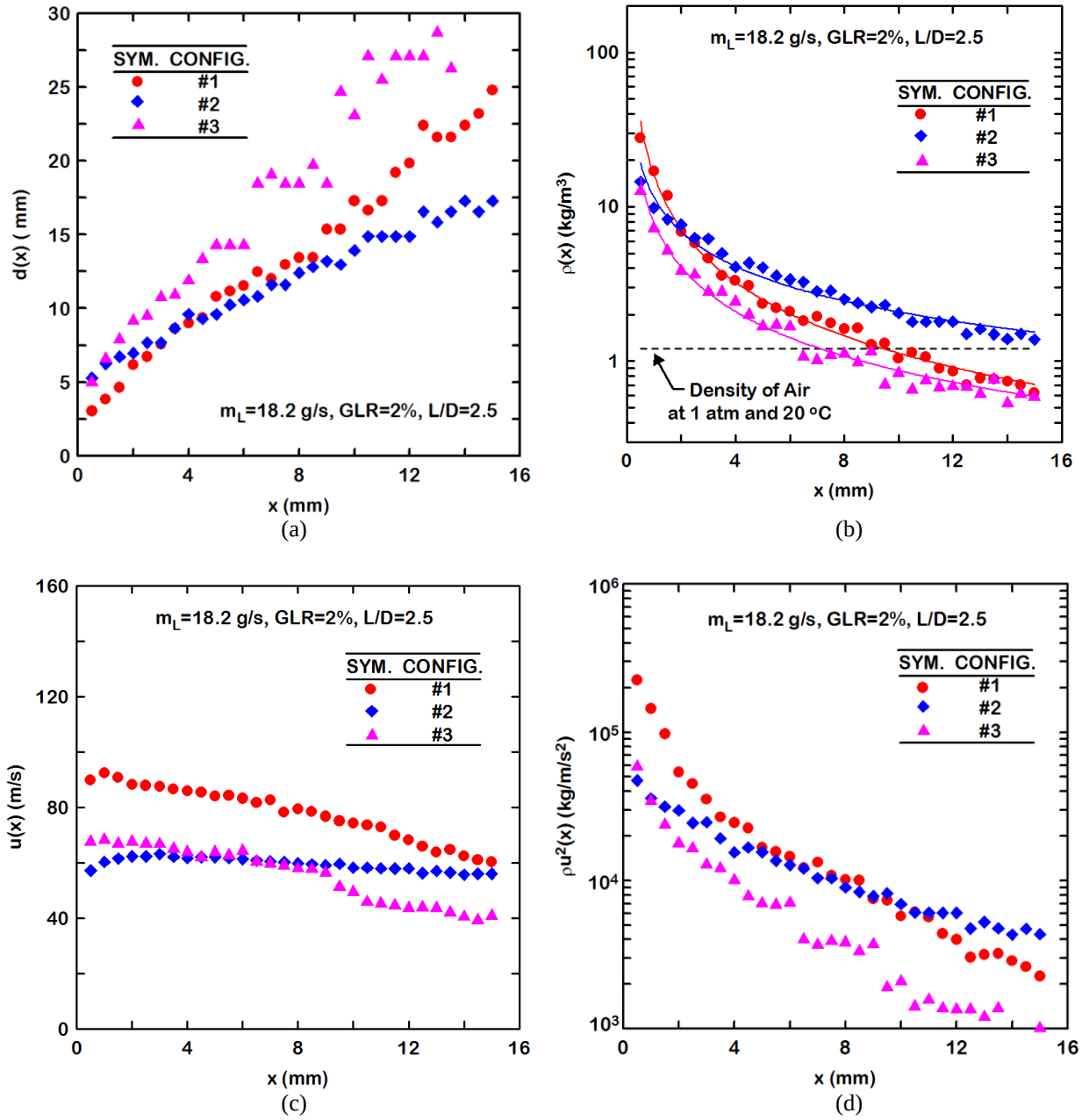

Figure 10. Axial distributions of (a) plume diameter, (b) weighted plume density, (c) weighted plume velocity, and (d) weighted momentum flux for aerated-liquid jets with various adaptor configurations at the same injection condition. L/D=2.5, m_L=18.2 g/s, GLR=2%.

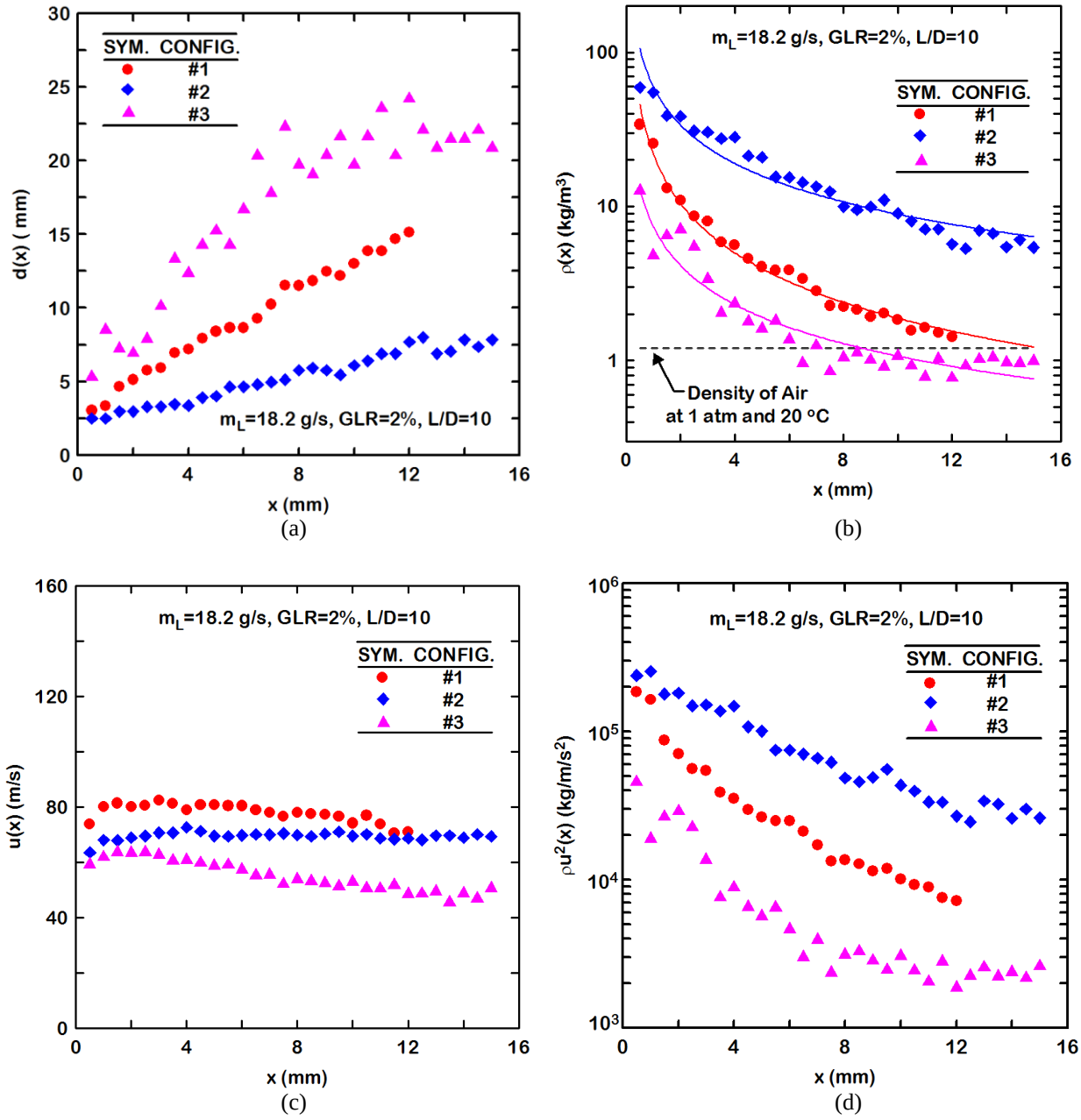

Figure 11. Axial distributions of (a) plume diameter, (b) weighted plume density, (c) weighted plume velocity, and (d) weighted momentum flux for aerated-liquid jets with various adaptor configurations at the same injection condition. L/D=10, m_L=18.2 g/s, GLR=2%.

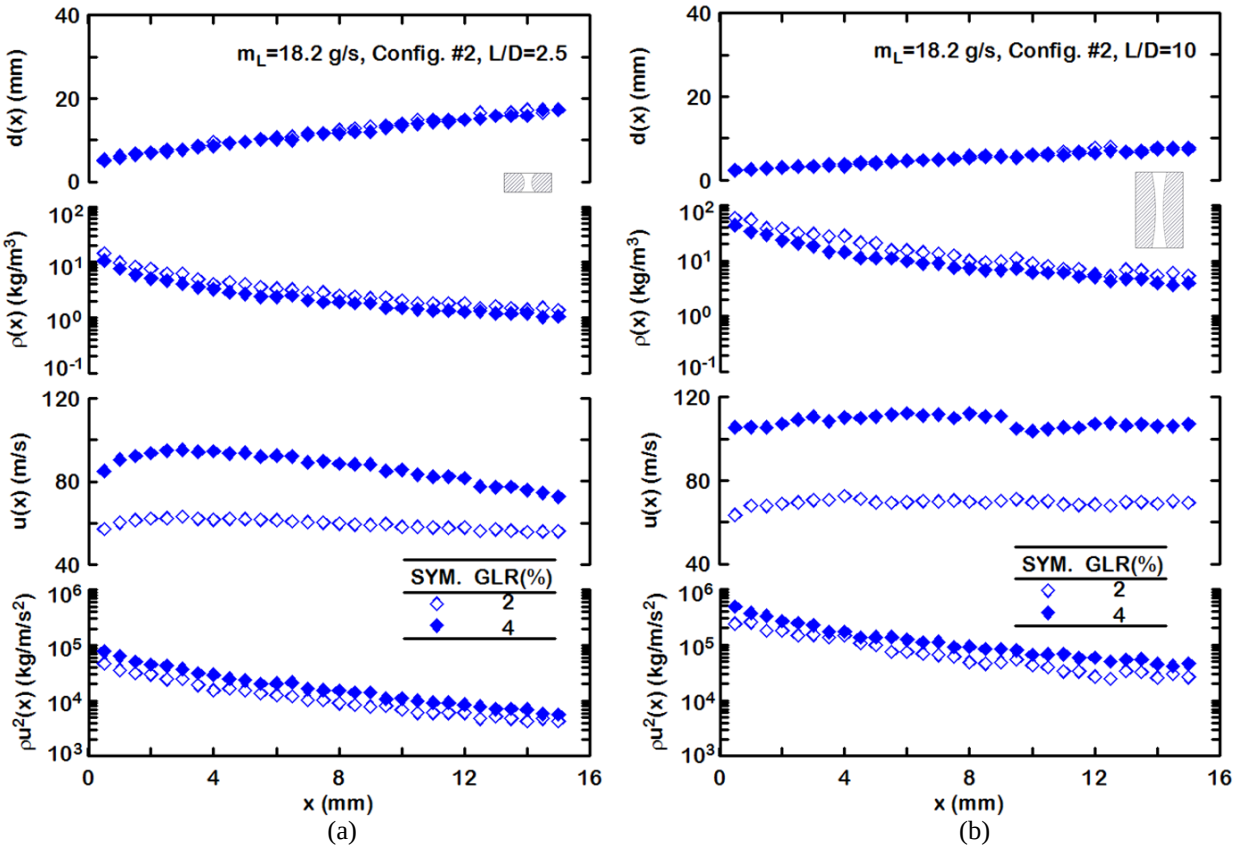

Figure 12. Axial distributions of plume properties, including diameter, weighted density, weighted velocity, and weighted momentum flux, for aerated-liquid jets with two adaptor lengths. Configuration #2, m_L=18.2 g/s, GLR=2% or 4%. (a) L/D=2.5, (b) L/D=10.